FED-Vol. 216, Unsteady Flows — 1995
ASME 1995

RECURRENCE OF BALLOON TREATED INTRACRANIAL TERMINAL ANEURYSM: A STUDY WITH PULSATILE BLOOD FLOW

Rupak K. Banerjee, Ph.D.
Young I. Cho, Ph.D.
Department of Mechanical Engineering and Mechanics
Drexel University, Philadelphia, PA 19104

Carlos F. Gonzalez, M.D.
Department of Radiology
Thomas Jefferson University Hospital
Philadelphia, PA 19107

ABSTRACT

To identify the hemodynamic mechanisms associated with recurrence of intracranial aneurysms following the treatment with balloon or coil occlusion. Pulsatile flow in a terminal recurrent intracranial aneurysm was numerically simulated based on the physiological pulsatile flow observed in the middle cerebral artery. In order to quantify the reason for recurrence of terminal aneurysm, flow parameters including local maximum wall shear stress and pressure drop at the neck of the aneurysm was calculated. Though the maximum shear stress at the right neck of the aneurysm after the insertion of the balloon is significantly reduced, it is still two and a half times more than the normal maximum shear stress. It is observed that due to the residual neck left after the insertion of the balloon an inadequate reduction in shear stress is achieved at the right neck where the recurrence of aneurysm is initiated. It is clear that the structural alteration of the endothelial layers in the aneurysm neck, where the shear stress was high, was critical.

INTRODUCTION

The traditional treatment for small aneurysms (berry) of the cerebral vessels is surgical clipping. Although effective, clipping includes open craniotomy, a long recovery and hospital stay, with potentially serious complications including operative or post-operative bleeding and severe spasm of the cerebral vessels. However, endovascular occlusion of aneurysms performed in the angiography room requires only a few hours with the patient ready for discharged within 48 hours after the procedure. Unfortunately about 20% of occluded aneurysms recur after the endovascular treatment. The early experience coupled with endovascular occlusion, along with its enormous benefits and advantages for patients, point to the need for a better understanding of the underlying mechanisms responsible for the recurrence and hence, develop improved procedures in order to prevent aneurysm recurrence.

An example of a recurrent aneurysm is shown in Figures 1a -1d. The angiogram of a middle cerebral terminal aneurysm of a patient without and with balloon occlusion, is shown in figures 1a and 1b respectively. The patient was originally treated by balloon occlusion with obliteration of the aneurysm (Fig. 1b). However, in an arteriogram performed two years after the original treatment, it is noted that there has been a recurrence of the aneurysm with a lobulated appearance (Fig. 1c). A subsequent embolization is performed using the detachable coil technique (Fig. 1d).

Reports of recurrent intracranial aneurysms from a narrow residual neck after incomplete surgical clipping are found in the neurosurgical literature. An analogous situation occurs in the endovascular treatment of aneurysms using detachable balloons or coils. Very often it is difficult to completely occlude the aneurysmal cavity leaving the distal and proximal wall of the neck partially uncovered due to the geometric configuration of aneurysms. This constitutes a significant problem because the recurrence of aneurysm often occurs at the partially exposed or uncovered neck of the aneurysm. It is more difficult to treat recurred aneurysm and the second procedure carries more risk to the patient than the first one. In the future this type of complication, in turn, may reduce or even preclude the use of endovascular technique for the treatment of intracranial aneurysms.

The response of the vascular endothelium to the hemodynamic stimuli (Gibbons and Dzau, 1994) such as arterial wall shear stress has been the object of increased interest in the development of aneurysms. Nature of flow in and around different types of aneurysms have been investigated by several researchers (Steiger, 1990). In general, the intra-aneurysmal flow pattern is primarily governed by the geometric relation between the aneurysm and the parent vessel. Steiger and Reulen (1986) observed flow instabilities at a Reynolds number of 300 during deceleration of flow in the glass model of a cerebral saccular aneurysm and concluded that the fluctuations in flow might induce vibration of the aneurysm wall and contribute to progression and eventual rupture of the aneurysm. Liepsch et al. (1987) conducted an in-vitro steady flow experiment and reported that the inflow into the aneurysm arose from the downstream lip and was directed toward the center of the fundus while the back flow to the parent vessel took place along the walls of the fundus. In a similar study, Steiger et al reported (1988, 1987) that the size of the aneurysm had no influence on the basic pattern of intra-aneurysm circulation. A quantitative estimate of flow parameters including wall shear stress, before and after balloon occlusion in a terminal aneurysm has not yet been documented.

Considering the above fact, the present study investigates the role of fluid flow parameters in a recurrent terminal aneurysm in a patient treated by balloon occlusion. Using angiographic data of the terminal aneurysm for both pre- and post-occlusion series, a numerical analysis with pulsed blood flow is conducted. In order to determine the cause of the recurrence, various flow parameters, including maximum wall shear stress before and after the obliteration of the aneurysm, are quantified.

METHODS

The objective of the present numerical study is to obtain the time-dependent solution of an incompressible, non-Newtonian fluid

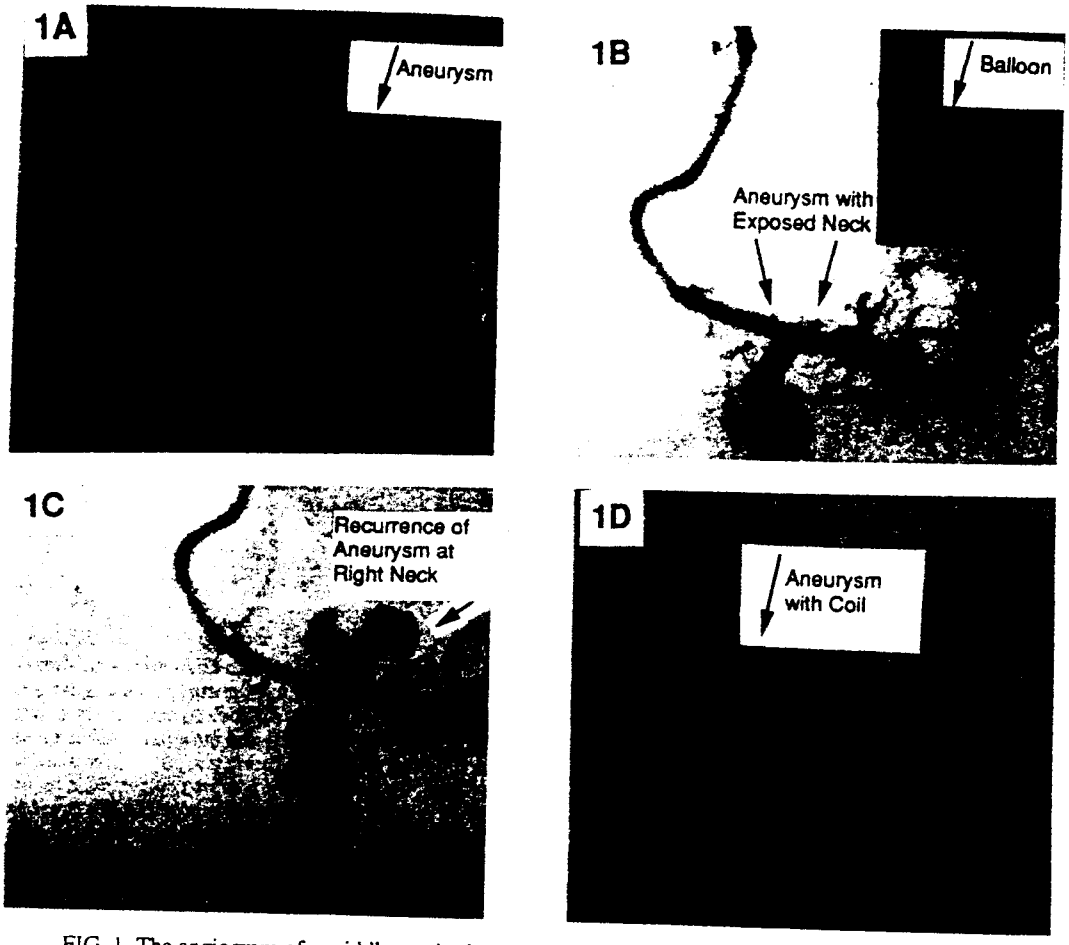

FIG. 1 The angiogram of a middle cerebral terminal aneurysm of a patient without (Fig. 1a) and with balloon occlusion (Fig. 1b). The balloon, after insertion, is shown as an in-set in Fig. 1b. Recurrence of the aneurysm, after two years, with a lobulated appearance (Fig. 1c). A subsequent embolization is performed using the detachable coil technique (Fig. 1d).

for selected geometry (Fig. 1a and 1b). The flow is described by the conservation equations of fluid mass and momentum. A finite element method (FEM) is used to solve the two conservation equations and thus to obtain the velocity, wall shear rate and stress, and pressure distributions. These two equations are presented as follows:

$$u_{i,i} = 0 \quad \text{, and} \qquad (1)$$

$$\rho\left[\frac{\partial u_i}{\partial t} + u_j u_{i,j}\right] = \sigma_{ij,j} + \rho f_i \qquad (2)$$

where i, j = 1, 2 for axisymmetric flows. u_i is the ith component of the velocity vector, ρ is density, σ_{ij} is stress tensor, and f_i is the body force.

The Galerkin formulation Baker (1983) using nine nodal quadrilateral elements is applied here in order to discretize the above continuity and momentum equations; this results in a set of nonlinear algebraic equations of the form

$$M\frac{du}{dt} + K(u)\,u = F \qquad (3)$$

where K(u) is the global system matrix developed from the momentum balance, M is the mass matrix, u is the unknown velocity, and F is the forcing function (including body forces and boundary conditions).

The mesh plot for the terminal aneurysm without and with balloon occlusion are shown in Fig. 2a and 2b respectively. The vessel diameter at the parent branch is d_1 = 3.8 mm, and at the daughter branches are d_2 = 3.6 mm and d_3 = 3.6 mm.

The matrix equation, representing a discrete analog of the original equations for an individual fluid element, is constructed, assembled and solved. For spatial integration, the number of iteration steps are limited to ten at each time step with a combination of the successive substitution and quasi-Newton scheme. The numerical simulation of a pulsatile flow requires a time integration method. The implicit time integration scheme used in the current study is the second-order trapezoidal method with a variable time step, which is dependent on the magnitude of temporal inlet velocity and its gradient change. Depending on the physiological velocity pulse shape, the time steps are varied between 1×10^{-4} to 1×10^{-5} s. The finite-element computer code FIDAP (1991) is used to formulate and solve this matrix equation. The IBM-3090 is used with TEMPLATE graphics for post-processing, and the results are down-loaded to an Apple-Macintosh II computer.

For validation of the numerical computation a procedure is adopted similar to the one described by Banerjee et al. (1993). The numerical calculations are performed for the center line instantaneous velocity and with uniform spatial inlet flow conditions. This is based on configuration of the short entry length of the parent artery. A typical *in-vivo* velocity profile at the core region of the middle cerebral artery, as measured by an ultrasound Doppler flow cuff, is used. The inlet velocity profile is normalized as shown in Fig. 3, and used as an input for the present numerical simulation. A no-slip boundary condition is specified on the rigid arterial wall.

In the present investigation, the Carreau model is used to

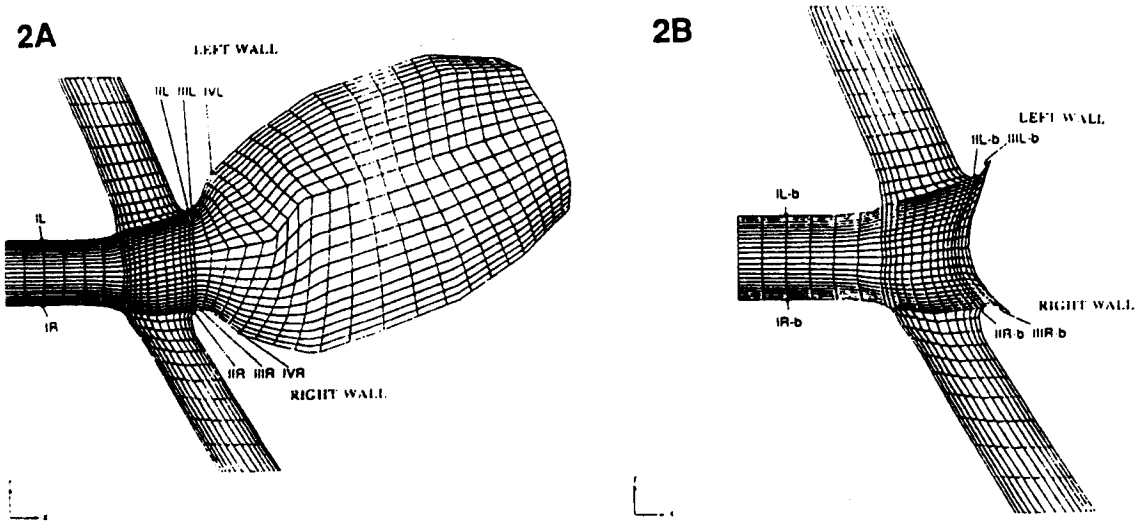

FIG. 2 The mesh plot for the terminal aneurysm without and with balloon occlusion are shown in Fig. 2a and 2b respectively. Figure 2b includes the residual neck as can be seen in Fig. 1b.

represent the shear rate dependent non-Newtonian blood viscosity whose model constants are obtained by curve-fitting of available shear-rate dependent blood viscosity data in the literature (Cho and Kensey, 1991)

$$\eta = \eta_\infty + (\eta_o - \eta_\infty)\left[1 + (\lambda\dot{\gamma})^2\right]^{\frac{n-1}{2}} \qquad (4)$$

where λ (characteristics time) = 3.313 s, n = 0.3568, η_o = 0.56 poise, η_∞ = 0.0345 poise. In order to calculate viscosity in the flow field locally, the local shear rate, $\dot{\gamma}$, is calculated from velocity gradient through the second invariant of the rate of strain tensor, $II_{\dot{\gamma}}$, as follows:

$$\dot{\gamma} = \sqrt{\frac{1}{2}\Pi} = \sqrt{\frac{1}{2}\left[\sum_i\sum_j \dot{\gamma}_{ij}\,\dot{\gamma}_{ji}\right]} \qquad (5)$$

After the local viscosity is determined using Carreau model, Eq. (4), the local shear stress, τ (= $\eta\,\dot{\gamma}$), is calculated. Blood with a constant density of 1.05 g/cm^3 and infinite shear rate kinematic viscosity ν_∞ ($=\eta_\infty/\rho$) are used in the calculations. The pulse rate is 75 bpm. Hence, the dimensionless frequency parameter [α = 0.5 d $(\omega/\nu)^{0.5}$] for the artery is found to be 4.87.

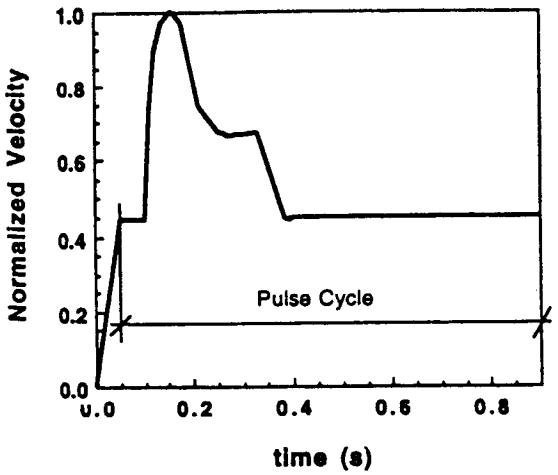

FIG. 3 Normalized form of the *in-vivo* velocity pulse in the middle cerebral artery.

RESULTS

This section includes spatial distribution of velocity, the temporal distribution of shear rate, non-Newtonian viscosity, shear stress and pressure drop during the systolic part of the pulse cycle. The flow calculations are presented for aneurysm with and without balloon. The diastolic part of the pulse is not reported here since insignificant change in flow parameters have been observed. In contrast, during the systolic part of the pulse, shown in Fig. 3, sharp changes in instantaneous velocity creates significant variations of calculated flow parameters.

Velocity Profile

At time step t= 0.105 s spatial distributions of axial velocity profiles, u_x, from the neck to the interior core of the terminal aneurysm are shown in Fig. 4. It is observed that the magnitude of velocity inside the core of the aneurysm is comparatively of a lesser order than the velocity in the main or daughter branch arterial velocities. The peak velocity in the main lumen is 44.6 cm/s whereas it is only 3 cm/s near the right neck of the aneurysm (locations IIR in Fig. 4). The nature of axial velocity profiles, u_x, indicate that the flow is positive at the core region whereas it is negative at the wall region of the aneurysm. This clearly shows that for a terminal aneurysm the flow enters through the core and leaves it along the aneurysm wall.

However, interestingly the axial flow distribution is asymmetric in nature and it is skewed more towards the right wall of the aneurysm. In other words when compared to the left wall of the aneurysm the peak velocity and sharper velocity gradient exist near the right wall region (locations IIR and IIIR in Fig. 4). The asymmetric distribution of the velocity is attributed to the geometric orientation i.e., angle between the aneurysm and the main and daughter arteries. It is most common to find asymmetric terminal aneurysm as compared to the symmetric ones.

Shear Rate

Figure 5A shows the magnitude of instantaneous shear rate at critical right wall locations (Fig. 2A) of the aneurysm prior to balloon treatment whereas Fig. 5B shows the shear rates at right wall for aneurysm following insertion of the balloon (Fig. 2B).

Plot No. 1R in Fig. 5A shows the normal instantaneous shear rate at the right wall location IR (Fig. 2A) during the systolic part of

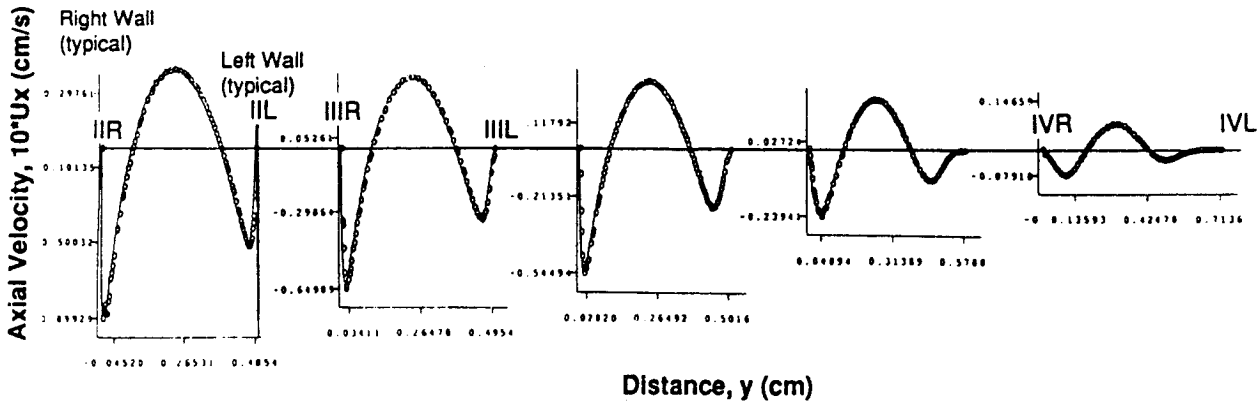

FIG. 4 At time step t= 0.105 s spatial distributions of axial velocity profiles, u_x, from the neck to the interior core of the terminal aneurysm.

the pulse cycle. The maximum normal shear rate of 1020 s^{-1} occurs at t= 0.16 s. Plot No. 2R in Fig. 5A shows the shear rate at the right neck location IIR (Fig. 2A) of the aneurysm. The maximum shear rate at the right neck of the aneurysm increased to a value of 5560 s^{-1} at t= 0.17 s which is more than 5 times the maximum value at location IR (arrow #1 in Fig. 5A). Plot No. 3R shows the shear rate at location IIIR (Fig. 2A) where the maximum shear rate is 1230 s^{-1} at t= 0.16 s. The instantaneous shear rate at this location reaches a value of the normal shear rate as observed for Plot No. 1R. As indicated by arrow #1 and #2 a phase shift has been observed where the time for maximum shear rate is different between Plot No. 1R and 2R. Shear rate at location IVR is insignificant since sharp reduction in flow occurs from location IR to IVR in the aneurysm sac. From the neck to the inside core of the aneurysm, the velocity gradient at the inside wall reduces and a stagnant flow region develops.

Because of the identical geometric location, Plot No. 1R-b in

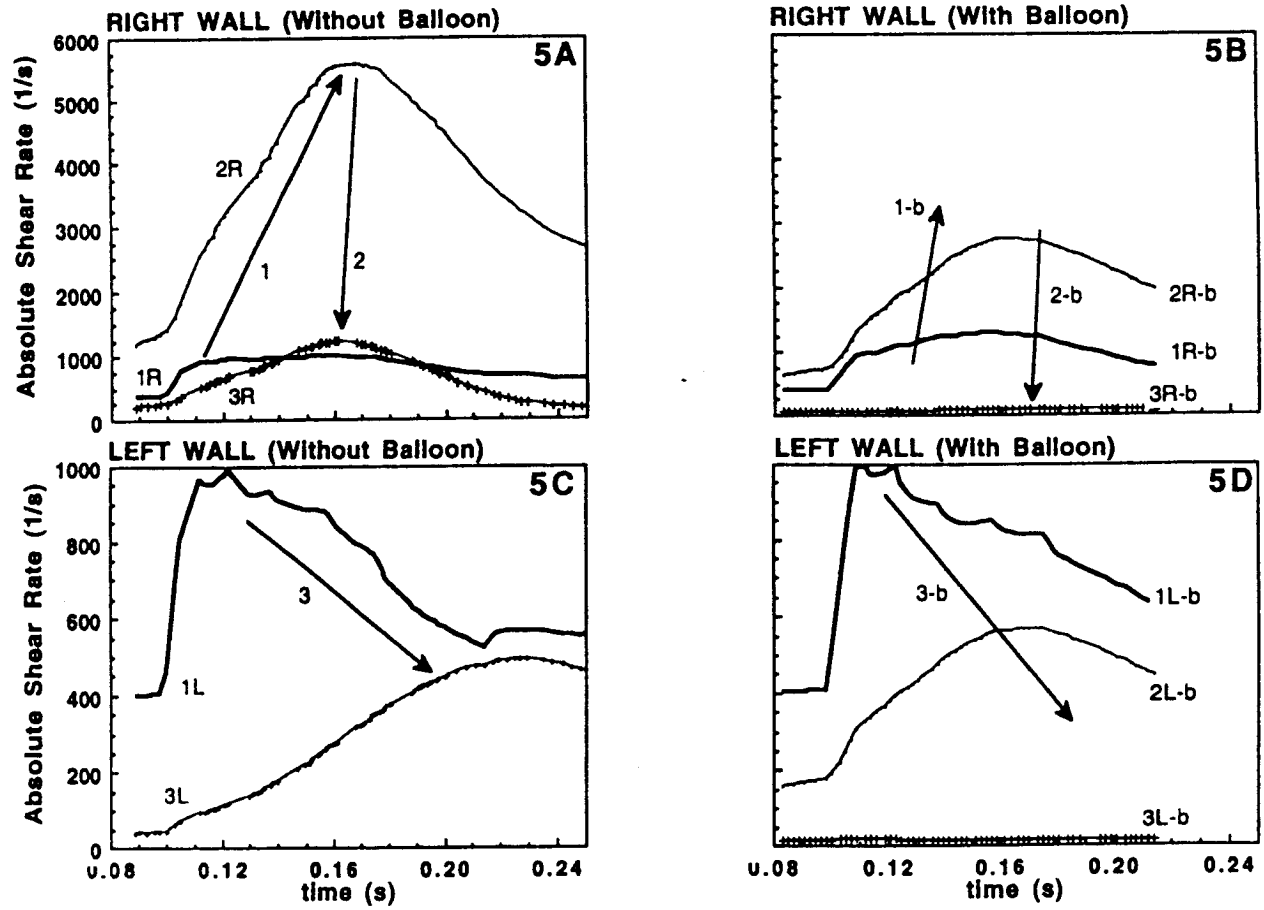

FIG. 5 Instantaneous shear rate at the right wall is shown in Fig. 5A for aneurysm without balloon and Fig. 5B for aneurysm with balloon and at the left wall is shown in Fig. 5C for aneurysm without balloon and Fig. 5D for aneurysm with balloon.

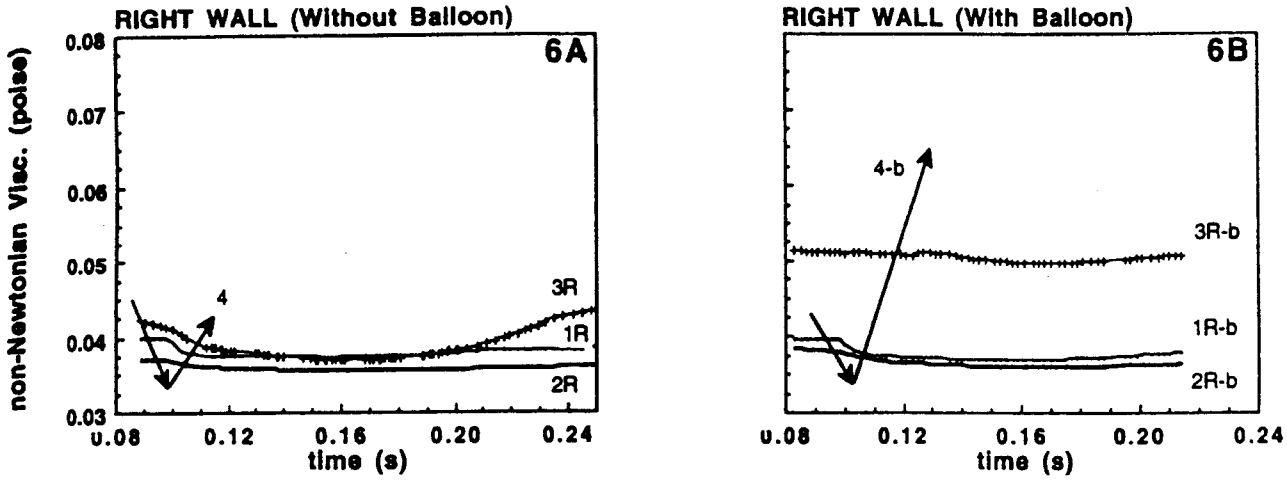

FIG. 6 Instantaneous non-Newtonian blood viscosity at the right wall is shown in Fig. 6A for aneurysm without balloon and Fig. 6B for aneurysm with balloon.

Fig. 5B shows similar temporal variation of normal wall shear rate as observed in Plot No. 1R in Fig. 5A. Plot No. 2R-b in Fig. 5B represent shear rate at the right neck of the aneurysm. The maximum shear rate at the right neck region with the inserted balloon is 2730 s^{-1} at t= 0.16 s (arrow #1-b in Fig. 5B) which is approximately half the maximum shear rate observed for the aneurysm without the balloon. It is evident that the maximum shear rate at the neck even with the balloon is approximately two and a half times the maximum normal shear rate obtained in location IR and IR-b in Fig. 2. The wall shear rate of the aneurysm close to the junction of the balloon wall is significantly less than the normal value as is observed in Plot No. 3R-b in Fig. 5B (arrow #2-b).

Plot No. 1L in Fig. 5C and Plot No. 1L-b in Fig. 5D show the normal instantaneous shear rate at the left wall locations 1L and 1L-b (Fig. 2). In general it is observed that the left wall shows reduced level of shear rate as compared to the normal value. The left wall of the aneurysm with and without balloon shows reduction in the magnitude of shear rate (arrow #3 and #3-b in Fig. 5C and 5D respectively). When compared to the maximum value of shear rate of 988 s^{-1} at t= 0.12 s (Plot No. 1L of Fig. 5C and 1L-b of Fig. 5D) the maximum shear rates for Plot No. 3L of Fig. 5C and 3L-b of Fig. 5D reduce to values of 429 s^{-1} at t= 0.23 s and only 18 s^{-1} at t= 0.10 s respectively. Clearly, reduction in shear rate has been observed at the left aneurysm wall with the balloon. Away from the neck, the inside wall of the aneurysm sac shows further reduction of shear rate. In addition, a phase shift has been observed between locations 1L to 3L of Fig. 5C and 1L-b to 3L-b of Fig. 5D.

Non-Newtonian Viscosity of Blood

Instantaneous value of non-Newtonian blood viscosity has been calculated at the right wall (Fig. 6A for aneurysm without balloon and Fig. 6B for aneurysm with balloon). The non-Newtonian blood viscosity is inversely dependent on the shear rate i.e., the blood viscosity is small at high shear rate whereas it is high at low shear rates.

For Plot Nos. 1R to 3R in Fig. 6A and Plot Nos. 1R-b to 3R-b in 6B the shear rate is generally high during the systolic part of the pulse cycle and specially, at the neck of the aneurysm where the blood shows infinite shear rate viscosity i.e., 0.0345 poise. Reduction in non-Newtonian viscosity of blood has been observed at peak systolic location since at this location the shear rate increases due to sharp increase in velocity gradient (arrow #4 and #4-b of Fig. 6A and 6B). The non-Newtonian viscosity is progressively higher from neck to the inside core of the aneurysm since the shear rate becomes significantly lower (as seen in Fig. 5A and 5B). When the balloon is inserted in the aneurysm the increase in blood viscosity is significant due to decrease in shear rate as can be observed from arrow #4 and #4-b of Fig. 6A and 6B.

Due to the sharper reduction of shear rate within a short distance the increase of non-Newtonian viscosity is much faster for the aneurysm with the balloon than without it. When compared with the left wall, the reduction in non-Newtonian viscosity for Plot No. 3R for Fig. 6A and Plot No. 3R-b for Fig. 6B is higher at the right wall. Since the change in shear rate dominates over change in non-Newtonian viscosity, the left wall data has not been presented here.

Wall Shear Stress

Based on the shear rate and non-Newtonian viscosity calculations in the previous sections, the shear stress is calculated. In this section the magnitude of maximum value of normal wall shear stress is compared with the shear stress at the aneurysm neck with and without balloon.

Table 1 shows that the normal value of the maximum shear stress calculated at the main inlet arterial wall is 37.7 dynes/cm^2. At the right neck (1R in Fig. 2A) of the aneurysm the maximum shear stress increases to a value of 194.6 dynes/cm^2. However, when the balloon is inserted in the aneurysm the maximum shear stress at the right neck (1R in Fig. 2B) decreases to a value of 98.3 dynes/cm^2. The shear stress calculations at the left neck (IL & IL-b in Fig. 2) is ignored since the magnitude of the shear rate at this location is significantly less than the right neck.

Table 1

Maximum wall shear stress at the right neck of the aneurysm.

	Normal	Without Balloon	With Balloon
Shear Rate (1/s)	1020	5560	2730
Viscosity (poise)	0.037	0.035	0.036
Shear Stress (dynes/sq. cm.)	37.7	194.6	98.3

Pressure

Instantaneous value of pressure drop has been calculated at the right wall (Fig. 7A for aneurysm without balloon and Fig. 7B for aneurysm with balloon). Since the aneurysm acts as a dead end, the flow significantly reduces which leads to a high pressure region inside the aneurysm sac. The pressure drop, when compared to the main inlet artery, increases from the neck region to the inside core of the aneurysm (arrow #6 in Fig. 7A). The right neck of the aneurysm without the balloon shows less pressure drop of about 1107 dynes/cm^2 at t= 0.18 s when compared with the core region of the aneurysm where the pressure drops is 1959 dynes/cm^2. When the balloon is inserted a reduction of maximum pressure drop from 1959 dynes/cm^2 to 1665 dynes/cm^2 is observed for the right wall of the aneurysm (arrow #7 and #7-b in Fig. 7A and 7B, respectively). A similar phenomenon is observed at the left wall of the aneurysms.

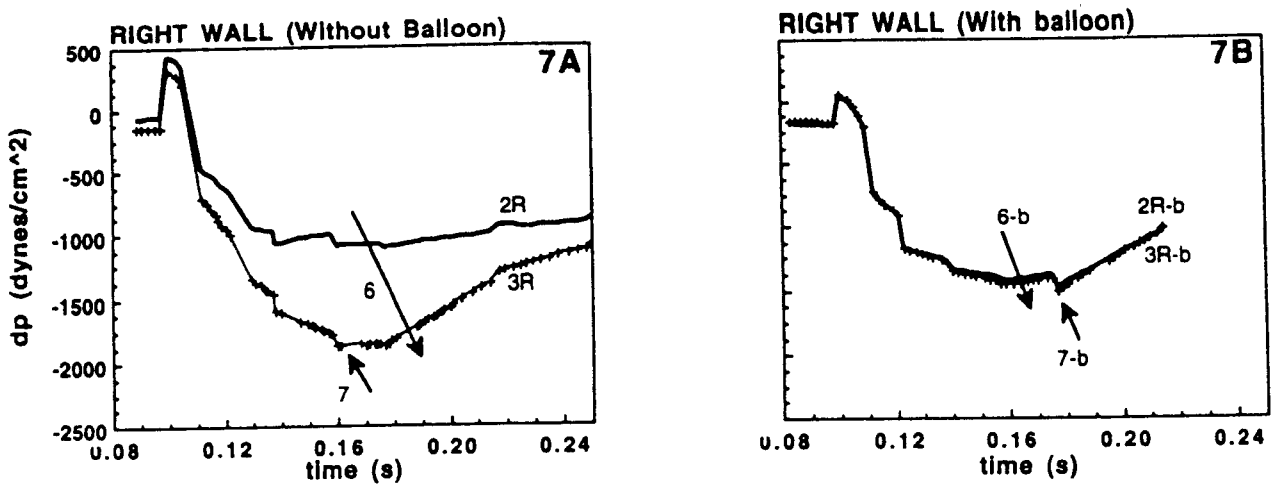

FIG. 7 Instantaneous pressure drop at the right wall is shown in Fig. 7A for aneurysm without balloon and Fig. 7B for aneurysm with balloon.

From Fig. 7A-7B, it is evident that the balloon helps in reducing the maximum pressure inside the aneurysm by approximately 15%.

DISCUSSION

A significant increase in shear stress occurs at the right neck of the aneurysm. It is calculated that, when compared to the normal maximum value of shear stress a five fold increase occurs at the right neck of the aneurysm without the balloon. However, when a balloon is inserted in the same aneurysm the maximum shear stress at the right neck decreases to half the value of the maximum shear stress calculated when the balloon was not inserted. Though the maximum shear stress at the right neck of the aneurysm after the insertion of the balloon is significantly reduced, it is still two and a half times more than the normal maximum shear stress calculated at the main inlet arterial wall.

The increased magnitude of localized wall shear stress is probably the primary hemodynamic factor responsible for the dilation of the neck, enlargement of the aneurysm and subsequent rupture of the sac before treatment. It is also evident that the existence of an elevated level of localized wall shear stress at the residual aneurysm neck seems to play a significant role in the recurrence, when aneurysms are not completely obliterated by conventional clipping or by endovascular occlusion of the sac.

Elevated level of shear stress causes injury and results in physiochemical changes in the endothelial cells at the neck location of the aneurysm wall which in turn may result in vascular remodeling (Gibbons and Dzau,1994). Vascular remodeling is an active process of structural alteration that involves changes in at least four cellular processes- cell growth, cell death, cell migration, and production or degradation of extracellular matrix - and is dependent on a dynamic interaction between locally generated growth factors, vasoactive substances, and hemodynamic stimuli. Active restructuring of the cellular and noncellular components of the vessel wall results in marked changes in luminal dimensions. Clinical examples of this form of remodeling include the vascular dilation associated with sustained high blood flow (e.g., an arteriovenous fistula) or the cell loss and matrix proteolysis that result in aneurysm formation.

SUMMARY AND CONCLUSION

The results and conclusion are summarized below:

1) Compared to the normal maximum value of shear stress a five fold increase occurred at the right neck of the aneurysm without the balloon.
2) When a balloon was inserted in the aneurysm the maximum shear stress at the right neck decreased to half the value of the maximum shear stress calculated without the balloon.
3) Though the maximum shear stress at the right neck of the aneurysm after the insertion of the balloon was significantly reduced, it was still two and a half times more than the normal maximum shear stress.
4) The balloon helped in reducing the maximum pressure inside the aneurysm by approximately 15%. However, the change in shear stress was significantly more than the pressure.
5) It was evident that due to the residual neck left after the insertion of the balloon an inadequate reduction in shear stress was achieved at the right neck of the aneurysm. Since the right neck of the aneurysm was not completely obliterated (Fig. 1b) the recurrence of aneurysm was initiated at the right neck, as can be seen in Fig. 1c. It is clear that the structural alteration of the endothelial layers in the aneurysm neck, where the shear stress was high, was critical.

REFERENCES

Baker, A. J., 1983 *Finite Element Computational Fluid Mechanics*, Hemisphere Publishing Corp.

Banerjee, R. K., Cho, Y. I., and Back, L. H. 1992, "Numerical Studies of 3-D Arterial Flows in Reverse Curve Geometry: Part I, Peak Flow," *ASME, Journal of Biomechanical Engineering*, Vol. 115, pp. 316-326.

Cho, Y. I., and Kensey, K. R., 1991, "Effects of the non-Newtonian Viscosity of Blood on Flows in a Diseased Arterial Vessel: Part 1, Steady Flows," *Biorheology*, Vol. 28, pp. 241-262.

FIDAP Manual, 1991, Fluid Dynamics International, Inc., Evanston, Illinois.

Gibbons, G. H., and Dzau, V. J., 1994, "The Emerging Concept of Vascular Remodeling," *The New England Journal of Medicine*, Vol. 330, No. 20, pp. 1431-1438.

Liepsch, D. W., Steiger, H. J., Poll, A., and Reulen, H. J., 1987, "Hydrodynamic Stress in Lateral Saccular Aneurysms," Biorheology, Vol. 24, pp. 689-710.

Steiger, H. J., 1990, "Pathophysiology of Development and Rupture of Cerebral Aneurysms," *Acta Neurochirurgica*, Springer-Verlag Wien, New York, Supplementum 48.

Steiger, H. J., Liepsch, D. W., Poll, A., and Reulen, H. J., 1988, "Hydrodynamic Stress in Terminal Saccular Aneurysms: A Laser-Doppler Study," *Heart and Vessels*, Vol. 4(3), pp. 162-169.

Steiger, H. J., Poll, A., Liepsch, D. W., and Reulen, H. J., 1987, "Basic Flow Structures in Saccular Aneurysms: A Flow Visualization Study," *Heart and Vessels*, Vol. 3(2), pp. 55-65.

Steiger, H. J., and Reulen, H. J., 1986, "Low Frequency Flow Fluctuations in Saccular Aneurysms," *Acta Neurochirurgica*, Vol 83 (3-4), pp. 131-137.